Astronomy & Astrophysics manuscript no. TYGAS_Ba
January 24, 2017

Hertzsprung-Russell diagram and mass distribution of barium stars

A. Escorza-Santos[1, 2], H.M.J. Boffin[3, 4], A.Jorissen[2], S. Van Eck[2], L. Siess[2], D. Pourbaix[2], H. Van Winckel[1], and D. Karinuzhi[2]

[1] Instituut voor Sterrenkunde, Katholieke Universiteit Leuven, Celestijnenlaan 200D, 3001 Leuven, Belgium
[2] Institut d'Astronomie et d'Astrophysique, Université Libre de Bruxelles, Campus Plaine C.P. 226, Boulevard du Triomphe, B-1050 Bruxelles, Belgium
[3] ESO, Alonso de Córdova 3107, Casilla 19001, Santiago, Chile
[4] ESO, Garching bei München, Germany

Received; Accepted

ABSTRACT

Still to come

Key words. Stars: binaries – .....

1. Introduction

Barium stars are a class of K giants with strong lines of elements like barium produced by the s-process of nucleosynthesis (Käppeler et al. 2011). Although the class was defined in 1951 (Bidelman & Keenan 1951), it is not until 1980 (McClure et al. 1980) that the origin of these overabundances were understood as the result of mass transfer in a binary system, the polluting heavy elements being formerly produced within an asymptotic giant branch (AGB) companion, now a very faint white dwarf (WD). The exact mode of mass transfer responsible for that pollution remained uncertain though, mainly because many barium systems are found in rather narrow orbits which could not accomodate an AGB star (Pols et al. 2003; Izzard et al. 2010, and references therein). Nevertheless, the WD nature of the companion is beyond doubt, thanks to the analysis of the orbital mass functions performed by Webbink (1988), McClure & Woodsworth (1990) and Van der Swaelmen et al. (2016), which reveal a peaked mass distribution for the companion, in accordance with expectation for WDs. The exact value of the WD mass depends of course upon the mass of the primary star (the barium star), which was so far difficult to derive with a good accuracy. Yet, the knowledge of the mass of the WD companion of barium stars would make a comparison possible with the average mass of field WDs (0.647 ± 0.014 $M_\odot$, from gravitational redshifts; Falcon et al. 2010). Any difference between the average mass of field and barium-companion WDs would then point to a signature of the mass-transfer process.

The mass of barium stars may be derived from their location in the Hertzsprung-Russell diagram (HRD), and from a comparison with evolutionary tracks. Mennessier et al. (1997) used a Bayesian method to infer barium-star masses, based on a HRD constructed from Hipparcos parallaxes. They conclude that mild and strong barium stars have somewhat different mass distributions, as mild and strong barium stars are characterised by masses in the range $2.5 - 4.5$ $M_\odot$ and $1 - 3$ $M_\odot$, respectively. The distinction between mild and strong barium stars is made on the "Ba index" introduced by Warner (1965), and reflects the strength of the Ba lines, based on visual inspection, on a scale from Ba1 to Ba5, Ba5 corresponding to the strongest lines. In this and our past studies, we associate Ba1 - Ba2 indices with mild barium stars and Ba3 - Ba5 indices with strong barium stars.

Thanks to the more accurate parallaxes provided by the Tycho-Gaia Astrometric Solution (TGAS; Michalik et al. 2015), it is possible to derive barium-star masses with a much better accuracy than it was possible with the Hipparcos data.

The location of barium stars in the HRD makes it possible as well to investigate the relation between that location and the orbital parameters. For instance, one may expect barium stars now residing in the He clump and which formerly went through the tip of the red giant branch (RGB), to exhibit a cutoff in their period distribution caused by the large radius reached at the RGB tip.

The paper is organized as follows: the TGAS sample is described in Sect. 2, and the method for deriving the atmospheric parameters in Sect. 3. The HRD diagram in then constructed in Sect. 4. The resulting mass distribution of barium stars is discussed in Sect. 5; the possible relationship between location in the HRD and orbital period is investigated in Sect. 6.

2. The sample

The sample has been constructed by selecting targets with Tycho-2 identifiers (Høg et al. 2000) in the barium star lists of Lü et al. (1983) and Lü (1991), in the list of CH and related stars of Bartkevičius (1996), and in the list of dwarf barium stars from North et al. (1994) and Edvardsson et al. (1993). These dwarf barium stars are collected in a compan-

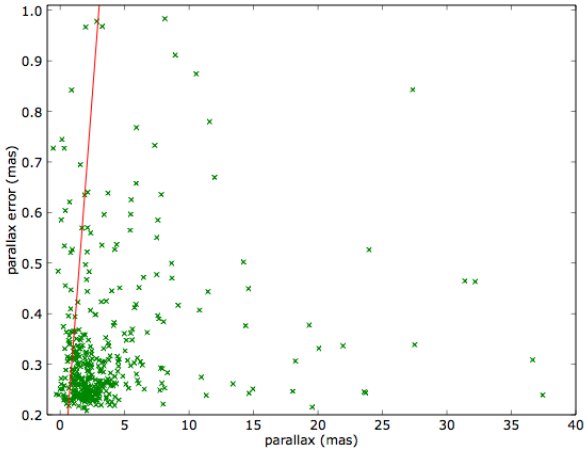

Fig. 1. The parallax and its error for the sample of barium stars and related objects studied in this paper. The red diagonal presents the threshold $\varpi/\sigma(\varpi) = 3$, below which stars are considered for inclusion in the HRD.

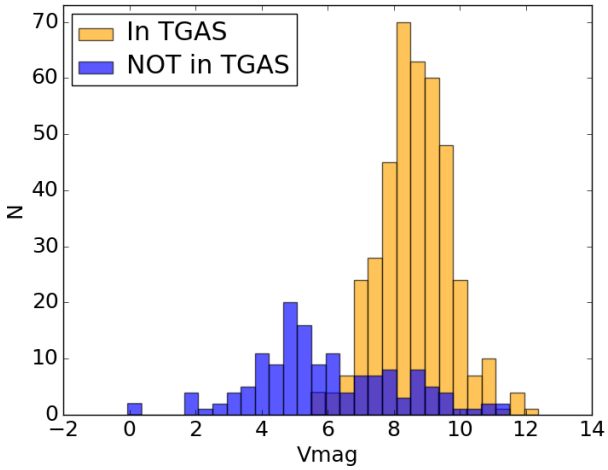

Fig. 2. The V magnitude distribution for stars in our sample present and absent from the TGAS catalogue.

ion paper (Escorza et al., in preparation) describing their orbital properties. The list of (dwarf and giant) barium, CH and related stars with a Tycho-2 identifier amounts to 546 entries. The TGAS catalogue (Michalik et al. 2015) provides a parallax value for 400 of them. We removed from the Bartkevičius (1996) list 11 high-proper-motion dwarf stars, labelled PM* by SIMBAD, for which we could not find any indication that they are either carbon or barium stars (like HD 208998, neither a carbon star nor a Ba star according to Bensby & Feltzing 2006; Bond et al. 2008). The list of stars removed for that reason comprises HD 11397, HD 15206, HD 24508, HD 89668, HD 108564, HD 145417, HD 153075, HD 154276, HD 161612, HD 164922, and HD 208998.

When the TGAS parallax was not available (as further discussed below), we used the Hipparcos parallax instead (ESA 1997, or the parallax rederived by Pourbaix & Jorissen 2000 in the case of 21 astrometric binaries), at least when the inverse relative parallax error $\varpi/\sigma(\varpi)$ exceeds 3, resulting in 114 Hipparcos entries. Applying the same quality selection on the TGAS parallaxes, we retain 336 stars. Our final list thus contains 450 entries.

Fig. 1 presents the relation between the parallax and its error for the complete sample of barium and related stars, before applying any quality selection. As described above and in Sect. 4, in order to build the HRD from a sample of stars with reasonably accurate parallaxes, we kept stars with $\varpi/\sigma(\varpi) \geq 3$; this limit is drawn as the red diagonal line in Fig. 1. Among 400 barium and related stars with a TGAS parallax, only 52 (13%) had to be rejected because they do not fulfill the accuracy criterion. No strong bias is expected from this small rejection rate, so that there is no need to discuss its impact on our results. We stress that in all the above, only the random error on the TGAS parallax has been considered. However, Michalik et al. (2015) indicate that a systematic uncertainty not larger than 0.3 mas might possibly add to the random uncertainty. This systematic uncertainty will nevertheless be considered below when estimating the uncertainty on the luminosity.

As shown in Fig. 2, the major cause for a star not be included in the TGAS catalogue is because it is brighter than $V \sim 6.5$. A small fraction of the fainter stars are missing as well. In an attempt to identify whether their absence in TGAS could be related their astrometric binary nature, stars with a missing TGAS parallax and a known orbital period (see Jorissen et al., in preparation) are listed in Table 1. In that Table, stars are ordered by increasing a_1/ϖ, the ratio between the angular semi-major axis of the astrometric orbit of the primary component around the center of mass of the system and the parallax. It may be estimated from Eq. (13) of Pourbaix & Jorissen (2000) which relies only on the masses and the orbital period:

$$\frac{a_1}{\varpi} = P^{2/3} \frac{M_2}{(M_1 + M_2)^{2/3}}, \quad (1)$$

where a_1/ϖ is in au while P is expressed in years and masses in $M_\odot$. It corresponds in fact to the semi-major axis of the absolute orbit of the primary component, expressed in au. In case the astrometric orbit has been detected from the Hipparcos data (Pourbaix & Jorissen 2000), that column provides the observed value. The observed value in principle corresponds to the orbit of the *photocentre* of the system around its centre of mass. However, since the cases considered here correspond to a WD companion, the photocentric orbit is identical to that of the primary component. If the astrometric orbit has not been seen in the Hipparcos data, the ratio a_1/ϖ is estimated from Eq. 1 by adopting $M_1 = 2.5$ $M_\odot$ and $M_2 = 0.62$ $M_\odot$, along with the observed orbital period.

A large a_1/ϖ value means that the binary motion is large with respect to the parallactic motion. If on top of a large a_1/ϖ value, the orbital period is close to 1 yr, the parallactic and binary motions will certainly be difficult to disentangle (Pourbaix & Jorissen 2000), a likely cause for the absence of the star in the TGAS catalogue. Among the fainter stars with no TGAS entries, several indeed have large a_1/ϖ values, but their orbital periods are often much larger than 1 yr. Moreover, since several systems with similar a_1/ϖ ratios (Pourbaix & Jorissen 2000) do have TGAS parallaxes (like HD 50264, HD 87080, HD 107574...), the orbital motion of the system does not seem to be the rea-

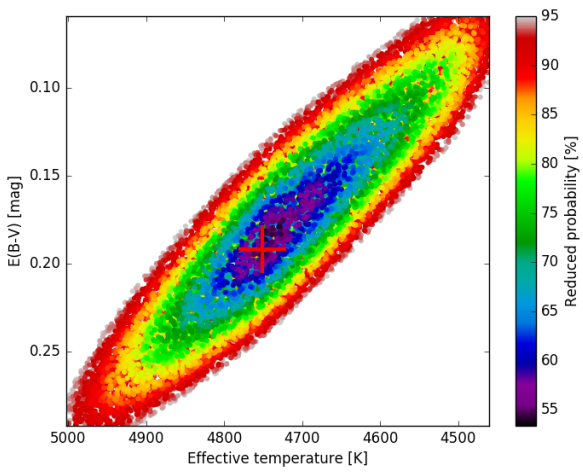

Fig. 3. The error ellipse resulting from the fit of the SED for star HD 183915, revealing the strong correlation between $T_{\rm eff}$ and E_{B-V}. The red cross identifies the best fit, predicting $E_{B-V} = 0.19$ whereas the selective extinction derived from Gontcharov (2012) for that star is $E_{B-V} = 0.225$ (leading to $A_V = 0.70$).

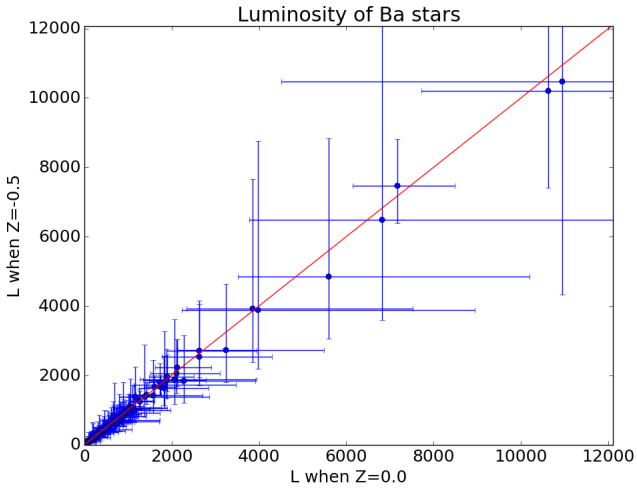

Fig. 4. The luminosities derived from SED fitting with models of solar metallicity or of metallicity [Fe/H]= −0.5.

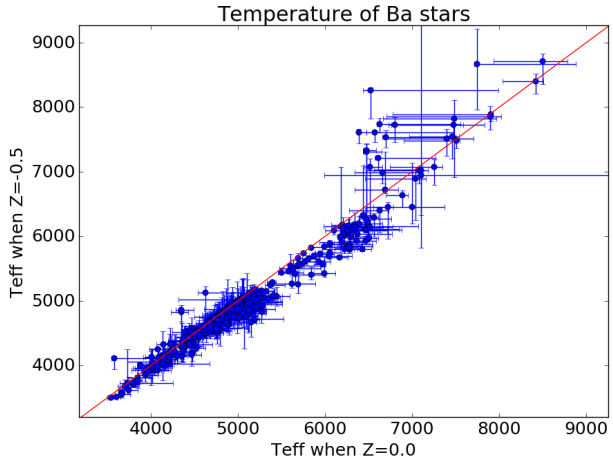

Fig. 5. Same as Fig. 4 for $T_{\rm eff}$.

son for its absence in the TGAS catalogue. At this stage, we cannot be sure of the exact reason for the absence of several faint barium and related stars in the TGAS catalogue, and the identification of this cause has to await the availability of the next data releases when quality flags of the Gaia astrometric solution will become available.

3. Atmospheric parameters

The atmospheric parameters of barium and related stars were derived by modelling the spectral energy distribution (SED) obtained by collecting magnitudes listed in the Simbad database. The best-fitting Kurucz model (Kurucz 1979) was obtained from a parameter-grid search using a χ^2 minimisation method (see Degroote et al. 2011, for details). The stellar temperature was then assigned from the best-fitting model and the luminosity was obtained by integrating the SED over all wavelengths spanned by the model, and applying the distance modulus derived from the parallax. The error bar on the luminosity is propagated from the parallax uncertainty (defined as the maximum between the random error and 0.3 mas, in an attempt to include the possible 0.3 mas systematic error on the parallax Michalik et al. 2015), and is thus asymmetric. The error on the temperature is the 1 sigma error enclosing 67% of the model fits (see Fig. 3).

The reddening $E_{\rm B-V}$ was initially left free during the fitting process. Its best value is estimated by looking for the amount of reddening to be applied to the Kurucz models in order to match the observed magnitudes. A value of 3.1 is used for the ratio of the total to the selective extinction $R = A_V/E_{\rm B-V}$ (Weingartner & Draine 2001), from which A_V is derived. In this process, we assume that the colour excess is the sum of interstellar and circumstellar reddening which are supposed to follow the same extinction law. It turned out that the temperature and extinction derived in this manner are strongly correlated, as shown in Fig. 3.

In a second run, the extinction was therefore fixed at the value computed by Gontcharov (2012), in his three-dimensional map of the extinction within the nearest kiloparsec. The location of the target in the Galaxy has been computed from its parallax. The resulting $T_{\rm eff}$ and E_{B-V} values were often found to fall at the edge of the 1σ ellipse error. It was therefore decided to let $E_{\rm B-V}$ vary freely between 0 and Gontcharov's value plus 0.07 mag. This prescription was found to lead to the most satisfactory results (see Fig. 3).

Finally, to evaluate the impact of the metallicity on the derived atmospheric parameters, two SED fits have been carried out, one imposing a solar metallicity, and another imposing [Fe/H] = -0.5. The resulting $T_{\rm eff}$ and luminosities are presented in Figs. 4 and 5, and reveal that the uncertainty introduced on these stellar parameters by the metallicity is negligible (the impact of the metallicity on the derived stellar *mass* is of course much larger, and will be discussed in Sect. 5).

Table 1. Barium stars not listed in the TGAS catalogue, and with a known orbital period (P), ordered by increasing a_1/ϖ values (see below). G is the Gaia magnitude and Ks is from the 2MASS survey (Skrutskie et al. 2006), ϖ is from the Hipparcos catalogue (ESA 1997) or from Pourbaix & Jorissen (2000) when available (PJ in column 'Rem.'). An asterisk in the 'Rem.' column means that the Hipparcos parallax has been used to locate the star in the HRD. Column a_1/ϖ is obtained from Pourbaix & Jorissen (2000) or from Eq. 1 for astrometric orbits not detected in the Hipparcos data.

HD/BD	TYC	V	G	$G-Ks$	ϖ(HIP) (mas)	a_1/ϖ (AU)	P (d)	Rem
Ba strong								
121447	6140-641-1	7.80	7.13	2.98	2.2 ± 1.0	0.2	186	
46407	5369-220-1	6.24	-	-	$6.6^{+1.3}_{-1.1}$	0.3	457	PJ,*
92626	8201-1209-1	7.09	6.67	2.25	$6.6^{+0.9}_{-0.6}$	0.5	918	PJ,*
NGC 2420 250	1373-1426-1	11.14	11.01	2.37	-	0.7	1404	
101013	3454-2188-1	6.124	-	-	$7.1^{+0.7}_{-0.6}$	0.8	1711	PJ,*
+38 118	2797-46-1	8.86	8.32	2.76	-	1.4	3877	
Ba mild								
77247	3805-1493-1	6.86	6.54	1.89	2.9 ± 1.0	0.1	80	*
218356	2239-1475-1	4.54	-	-	6.1 ± 0.7	0.1	111	*
288174	119-1058-1	9.02	-	-	2.9 ± 1.3	0.8	1818	
204075	6372-1278-1	3.74	-	-	$8.6^{+1.1}_{-1.0}$	1.0	2378	PJ,*
131670	4999-334-1	8.01	7.62	2.31	2.3 ± 1.2	1.2	2930	
139195	933-1240-1	5.26	-	-	13.9 ± 0.7	1.7	5324	*
53199	761-980-1	9.07	8.79	1.79	3.7 ± 1.3	2.3	8300	*
51959	4813-1015-1	8.92	8.61	2.07	6.5 ± 1.3	2.5	9488	*
104979	866-1180-1	4.12	-	-	19.1 ± 0.8	3.3	13940	*
98839	3015-2321-1	5.03	-	-	6.6 ± 0.6	3.7	16419	*
119185	5552-1079-1	8.91	8.57	2.02	3.9 ± 1.1	4.1	19467	*
Ba dwarf								
76225	6580-2586-1	9.20	-	-	3.4 ± 1.1	1.0	2411	*
89948	6631-715-1	7.55	7.31	1.12	23.4 ± 0.9	0.7	667.8	PJ,*
98991	6088-2156-1	5.09	-	-	22.0 ± 0.8	1.1	2834	*
221531	5832-970-1	8.36	8.21	0.98	$9.6^{+1.4}_{-1.3}$	1.2	1416	PJ,*
95241	3012-2522-1	6.03	-	-	22.0 ± 0.8	1.8	5448	*

4. The Hertzsprung-Russell diagram

The HRD has been constructed from the effective temperatures and luminosities obtained as described in Sect. 3. Fig. 6 shows the HRD for parameters obtained by leaving the extinction free (between 0. and Gontcharov's value), and by restricting the sample to stars with $\varpi/\sigma(\varpi) \geq 3$. Typical error bars are shown for two situations: a favourable one (left: $\varpi/\sigma(\varpi) = 8$), and the limiting case for $\varpi/\sigma(\varpi) = 3$ (right). In the latter case, the asymmetric nature of the errors on the luminosity (e.g., Luri & Arenou 1997) starts to be noticeable, so that biases will manifest (e.g., Luri & Arenou 1997). However, as apparent on Fig. 1, the number of targets located beyond the $\varpi/\sigma(\varpi) = 3$ threshold is not large, and a discussion on the effect of the biases does not seem to be required here. The STAREVOL evolutionary tracks corresponding to solar metallicity $Z = 0.0134$ have been superimposed (Siess 2006), for models of masses 1.0, 2.0, 3.0, 4.0, 5.0 and 6.0 $M_\odot$, as labelled. Fig. 7 shows the impact of metallicity for the STAREVOL tracks of 2.0 and 3.0 $M_\odot$ (black and red tracks, respectively). It appears that the [Fe/H] = -0.5 track of 2.0 $M_\odot$ covers the same region as the [Fe/H] = 0. track of 3.0 $M_\odot$; there is thus a strong degeneracy in the mass determination of a given star, that can only be lifted by knowing its metallicity.

It appears that several among the stars from the list of Lü et al. (1983) and Lü (1991) are in fact barium dwarfs or subgiant CH stars. They are listed in Table 2, and were selected from the criterion $L \leq 10 L_\odot$. The table contains as well a few dwarf Ba or carbon stars from the catalogue of Bartkevičius (1996).

A strong concentration of barium stars is found in the He clump, corresponding to evolutionary tracks for stellar masses between 2 and 3 $M_\odot$. The corresponding mass distribution is investigated in Sect. 5.

For comparison, Fig. 8 presents the HRD for S stars, from Shetye et al. (in preparation). As expected, extrinsic (Tc-no) S stars appear to be the counterparts of barium stars at lower temperatures.

Early R-type carbon stars are another family of peculiar stars with a strong concentration in the He clump (Knapp et al. 2001).

Table 2. A list of dwarf barium stars, not previously recognized as such, from the catalogues of Lü et al. (1983), Lü (1991), and Bartkevičius (1996).

Name	TYC	Ref.	Rem.
HD 8270	8036-564-1	Lü (1991), dwarf nature confirmed by Pereira (2005)	
HD 13551	8851-37-1	Lü (1991), dwarf nature confirmed by Pereira (2005)	
HD 22589	4722-19-1	Lü (1991), dwarf nature confirmed by Pereira (2005)	orbit available
CpD -44 5038	7735-447-1	Lü (1991)	
BD -10 4311	5630-641-1	Lü (1991)	orbit available
HD 197481	7457-641-1	Lü (1991)	
CS 22180-0013	5279-303-1	Bartkevicius	
HIP 19050	1814-348-1	Bartkevicius, classified as R	
HD 175179	5123-323-1	Bartkevicius PM*, moderate enhancement (0.2 – 0.3 dex of Y and Ba) (Bensby et al. 2014)	

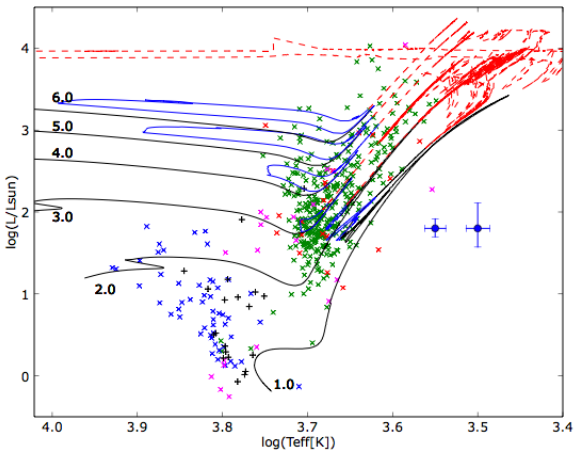

Fig. 6. The HRD for the sample of barium stars (green crosses: barium stars; blue crosses: barium dwarfs) and related objects (red crosses: CH stars; black plusses: subgiant CH stars; magenta crosses: carbon stars from the list of Bartkevičius (1996)) studied in this paper. Typical error bars are shown (as blue dots) for two situations: a favourable one (left: $\varpi/\sigma(\varpi) = 8$), and the limiting case for $\varpi/\sigma(\varpi) = 3$ (right). Stellar tracks from the STAREVOL code (Siess 2006) have been overplotted and correspond to solar metallicity $Z = 0.0134$, for models of masses 1.0, 2.0, 3.0, 4.0, 5.0 and 6.0 $M_\odot$, as labelled. The black tracks to the post-main-sequence phase up to the tip of the RGB (low-mass stars) or to the onset of core He-burning (intermediate-mass stars), blue tracks to core He-burning, and red dashed tracks correspond to the early and thermally-pulsing AGB (TP-AGB).

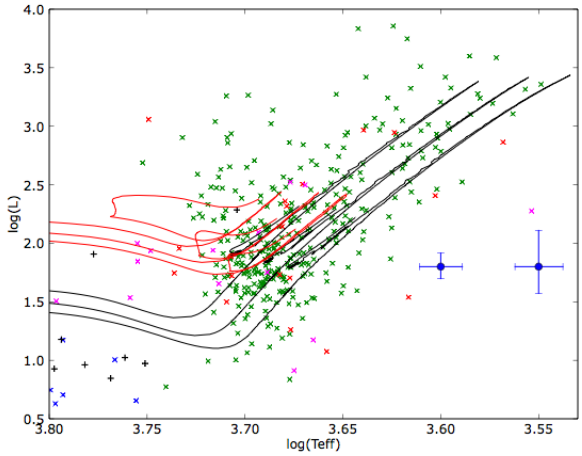

Fig. 7. Same as Fig. 6 for the STAREVOL 2.0 and 3.0 $M_\odot$ (black and red tracks, respectively) evolutionary tracks (Siess 2006), showing the impact of metallicity (from top to bottom: [Fe/H] = -0.5, -0.2 and 0).

5. Mass distribution

Fig. 10 presents the mass distribution of giant barium stars, from their location in the HRD and a comparison with the Padova evolutionary tracks corresponding to the metallicity closest to the one listed in the literature for the considered star **Refer to the master table******. The mass distribution appears strongly peaked in the range 2.0 - 2.5 $M_\odot$, and this peak is superimposed on a broader distribution extending from 1 to 5 $M_\odot$. To evaluate the sensitivity of these numerical values to the assumptions underlying the evolutionary tracks, a mass distribution has been computed as well with the STAREVOL tracks, and the result is ..... (Fig. 11).

We compare the situation prevailing for barium stars with that in the comparison sample of 5952 K and 739 M giants from Famaey et al. (2005), restricting the sample to the generic kinematical groups 'Background' (B) and 'Young' (Y). Famaey et al. (2005) performed a Bayesian classification of this large sample into different kinematical groups, based not only on their kinematics (Tycho-2 proper motions and CORAVEL radial velocities; Høg et al. 2000; Baranne et al. 1979, respectively) but also on their luminosity (derived from a Bayesian estimate based on the Hipparcos parallax). The B group constitutes the smooth velocity ellipsoid, whereas the Y group exhibits all signatures of young stars (small velocity dispersions and scale height; high luminosity, hence mass). To locate the stars in the HRD with $T_{\rm eff}$– L axes as for barium stars, it was necessary to use various calibrations from Bessell et al. (1998), notably $(V-I, V-K)$ and $(V-K, T_{\rm eff})$ to convert Hipparcos $V-I$ indices into temperatures, and $(V-K, BC_K)$ to convert visual absolute magnitudes into luminosities. The

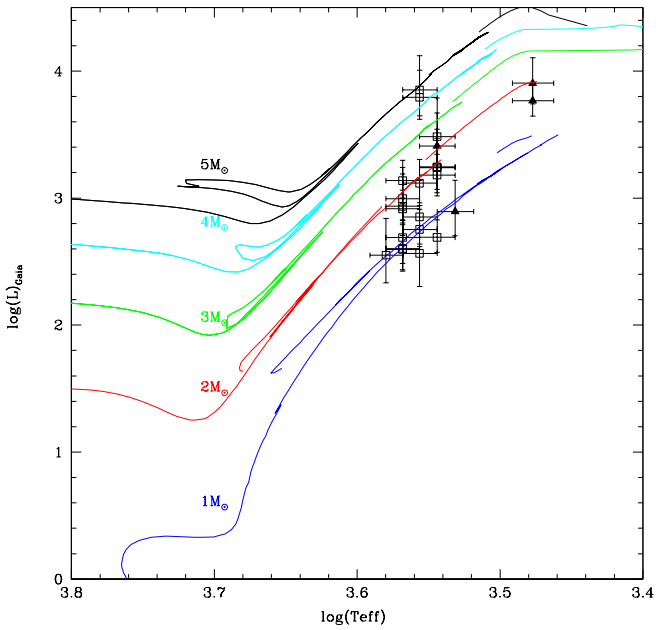

Fig. 8. The HRD for S stars, from Shetye et al. (in preparation). Extrinsic (Tc-no) and intrisic (Tc-yes) S stars are displayed as open and filled symbols, respectively.

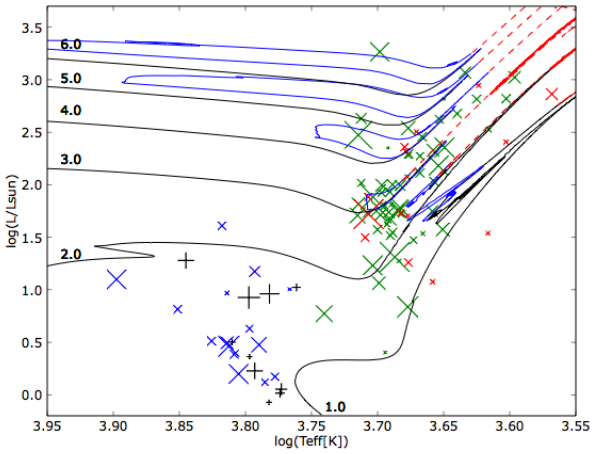

Fig. 9. Same as Fig. 6, but with the symbol size proportional to the orbital period.

resulting HRD is shown in Fig. 12, and a strong concentration is found in the He clump of stars with masses in the range 2 – 3 $M_\odot$. The corresponding mass distribution is shown in Fig. 13, which reveals that barium stars and their comparison sample of normal K and M giants behave similarly in terms of mass. The strong concentration of barium stars around 2.5 $M_\odot$ should thus be considered as a result of a population effect in the Galaxy.

6. Location in the HRD and orbital period

Fig. 9 is a first attempt to correlate the location of a binary system in the HRD with its orbital period. There is a clear trend to find large orbital periods for systems with the primary component located in the He clump, as compared to systems lying below the He clump (i.e., with luminosities from the main sequence up to the He clump). In an attempt to quantify this effect, the sample has been split in two subsamples: one with $\log L/L_\odot \leq 1.5$ ($L/L_\odot \leq 31.6$, and the other with $1.5 < \log L/L_\odot \leq 2.2$ ($31.6 < L/L_\odot \leq 160$). The first sample comprises main-sequence and subgiant stars whose current primary components never climbed the red giant branch (RGB), whereas the second comprises systems

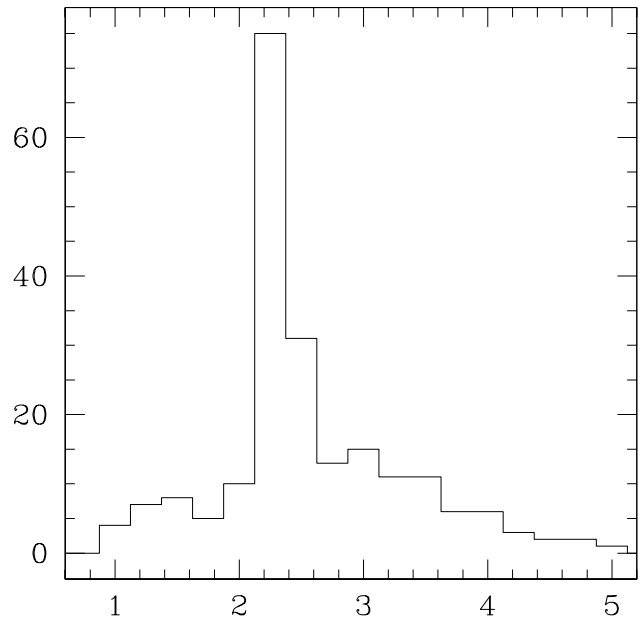

Fig. 10. The mass distribution for barium stars, from a comparison with the Padova evolutionary tracks.

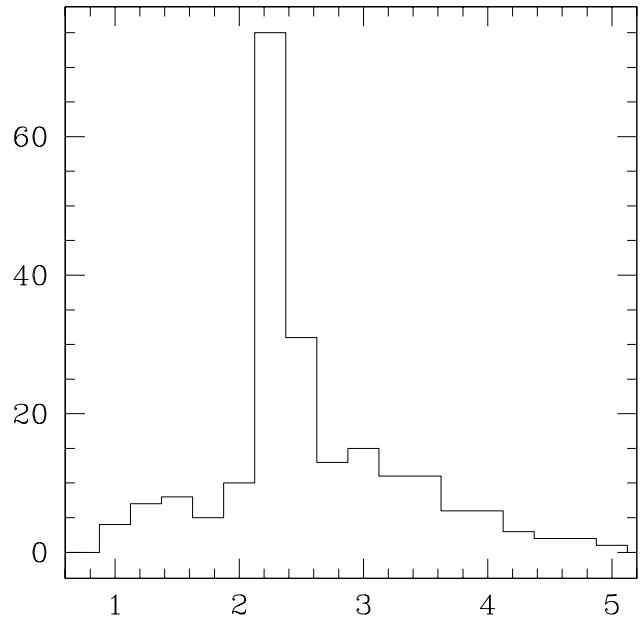

Fig. 11. The mass distribution for barium stars, from a comparison with the STAREVOL evolutionary tracks. ****** Still to be updated******

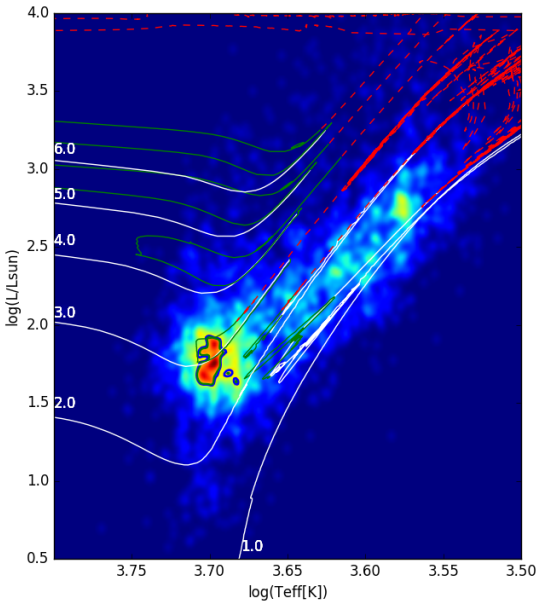

Fig. 12. The distribution of a comparison sample of K and M giants from Famaey et al. (2005) in the HRD. The data are presented as a contour density plot. STAREVOL evolutionary tracks for solar-metallicity stars with initial masses 1, 2, 3, 4, 5, and 6 $M_\odot$ (from bottom to top) are superimposed on the data (white colours correspond to Hertzsprung-gap and RGB evolution, green colours to core He-burning and red to AGB evolution). Stars from the Y group correspond to the faint extension of the stellar density in the regions covered by the 4, 5, and 6 $M_\odot$ evolutionary tracks.

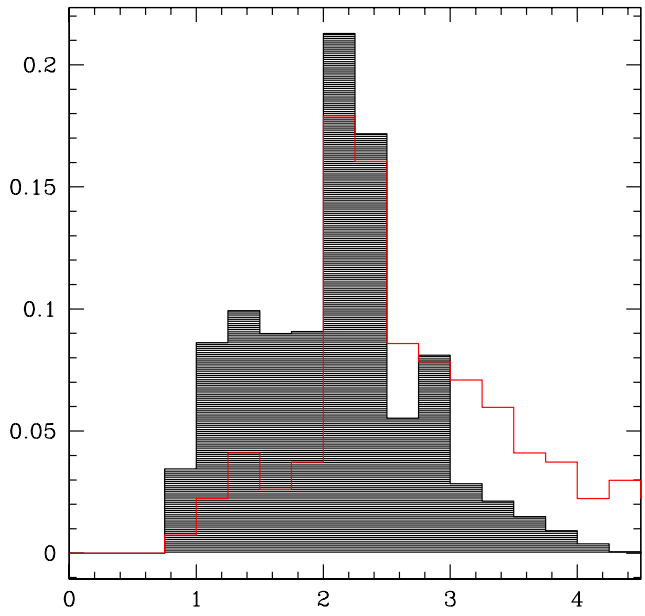

Fig. 13. Same as Fig. 11 (Barium stars in red) for the comparison sample of K and M giants (hatched histogram) from Famaey et al. (2005). **** Add the Y group !! *****

in the He clump after their passage through the RGB tip (at least for systems with low-mass primaries) and a few less evolved objects (on their way to the RGB tip). Given the involved timescales, the second category is likely a minority of the second subsample. Given the large radius reached at the RGB tip (see below), one may suspect that the giant filled its Roche lobe in the closest systems, which possibly evolved through a common-envelope stage into a system with properties that would not flag it any longer as a barium star but rather as a cataclysmic variable or even a coalesced pair. Fig. 15 confirms that very few systems ($7/38 = 18\%$) located in the He clump have periods shorter than 1000 d (those could in fact be pre-RGB systems). Compared to the pre-RGB systems (blue histogram and cumulative distribution in Fig. 15), there is indeed a clear deficit of short-period systems among clump He stars.

We demonstrate in Table 3 that the 1000 d period threshold is indeed set by the radius reached at the RGB tip. From the radius at the RGB tip, we compute the corresponding radius a of a circular orbit, assuming that the giant star fills its Roche lobe. We use the simplified relation from Livio (1994):

$$R_R = a(0.38 + 0.2 \times \log q), \quad (2)$$

where $q = M_1/M_2$, where M_1 is the mass of the giant star, and M_2 that of its WD companion, assumed to be equal to 0.62 $M_\odot$.

This segregation in terms of orbital periods between pre-He-clump and He-clump systems requires further investigation, since even pre-He-clump stars had progenitors that went through the thermally-pulsing AGB (TP-AGB), which involves as well stars with very large radii that should suppress as well short-period systems, as observed for post-RGB systems. To quantify this effect, the critical orbital periods corresponding to Roche-lobe-overflow at the AGB and RGB tips have been computed from the STAREVOL tracks. They obey the following relations:

$$R_{R,1}/A \equiv f = 0.38 + 0.2 \log(M_1/M_2), \quad (3)$$

and

$$P = \frac{(R_{\rm tip}/f)^{3/2}}{(M_1 + M_2)^{1/2}}, \quad (4)$$

where P is the critical period expressed in years, $R_{\rm tip}$ the radius reached at either the RGB or AGB tip (expressed in au, and identified with the Roche radius $R_{R,1}$), and $M_{1,2}$ the component masses expressed in $M_\odot$. $R_{R,1}$ is the critical Roche radius around the (overflowing) component of mass M_1. Three different critical periods must be considered: (i) $P_{\rm RGB,1}$, reached when the initially more massive component (now a WD) reaches the RGB tip (then in the above equations, $M_1 = M_{1@RGBtip}, M_2 = M_{\rm Ba}$), (ii) $P_{\rm AGB,1}$, reached when the initially more massive component (now a WD) reaches the AGB tip (then $M_1 = M_{1@AGBtip} = M_{\rm WD}, M_2 = M_{\rm Ba}$), and (iii) $P_{\rm RGB,2}$, reached when the initially less massive component (the current barium star) reaches the RGB tip, its companion being a WD (then $M_1 = M_{\rm Ba}, M_2 = M_{\rm WD}$). A supplementary condition is that the barium-star mass ($M_{\rm Ba}$) is smaller than the initial mass of its companion, the WD progenitor (to ease the computations, we neglected the mass transferred onto the barium star). The results are displayed in Fig. 16.

It is clearly seen that RLOF at the RGB tip occurs for all systems with periods shorter than 500 d for low-mass

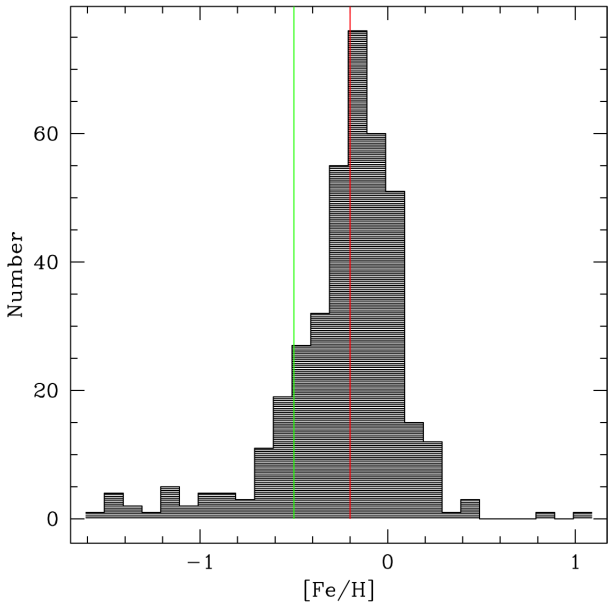

Fig. 14. Metallicity distribution for barium stars, from the literature.

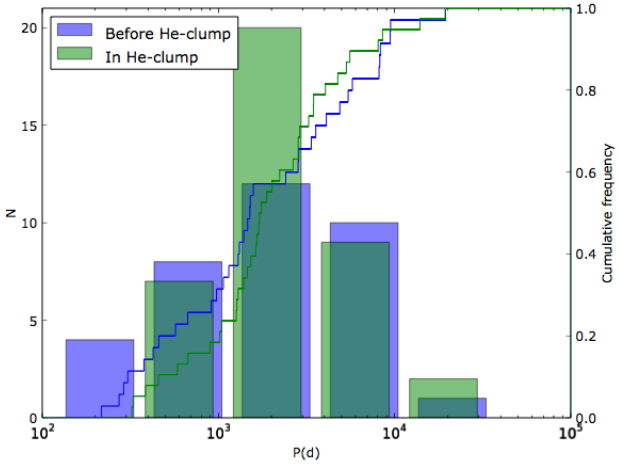

Fig. 15. The histogram (left scale) and cumulative frequency distribution (right scale) for orbital periods of barium and related systems. Systems with $\log L/L_\odot \leq 1.5$ ($L/L_\odot \leq 31.6$) are depicted in blue, and systems with $1.5 < \log L/L_\odot \leq 2.2$ ($31.6 < L/L_\odot \leq 160$) are depicted in green. The bins have a width of 0.5 in logarithmic scale.

stars (smaller than 1000 d for 1 $M_\odot$ stars; see also Table 3). For intermediate-mass stars ($2.5 < M/M_\odot < 8$), which do not evolve along an extended RGB, the radius stays small, so that the critical period is too short to be of any relevance for the current discussion. Clearly, the threshold for low-

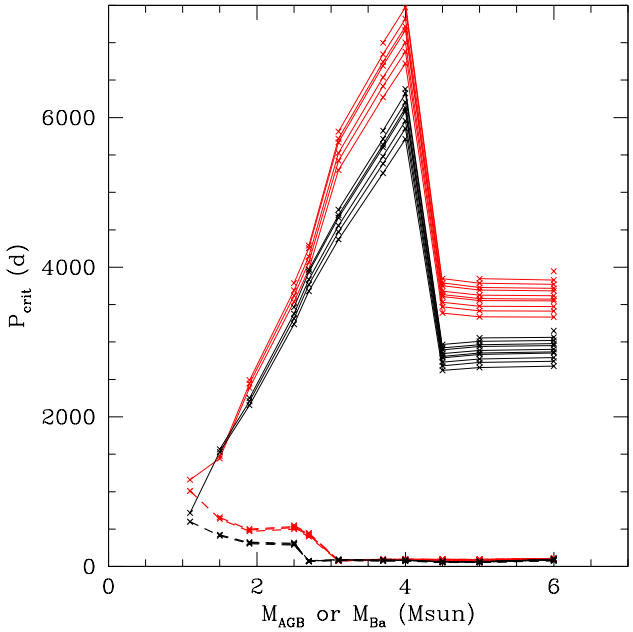

Fig. 16. The critical periods below which one of the components fills its Roche lobe at either the tip of the RGB ($P_{\rm RGB,1}$, see text; thick dashed line) or at the tip of the AGB ($P_{\rm AGB,1}$, thin solid line). The input data $R_{\rm RGB,tip}$ and $R_{\rm AGB,tip}$ are taken from the STAREVOL grid (red curves: solar metallicity $Z = 0.0134$; black curves: [Fe/H]$= -0.5$ or $Z = 0.0043$). The different lines in a series correspond to different barium-star masses (1.1, 1.5, 1.9, 2.5, 2.7, 3.1, 3.7, 4., 4.5, 5 and 6 $M_\odot$). For a given barium-star mass, the AGB component is necessarily more massive. Therefore, the different lines have different lengths: they start at $M_{\rm Ba}$, and comprise all AGB stars more massive than the starting $M_{\rm Ba}$ value. The critical period $P_{\rm RGB,2}$ (see text) does not strongly depend upon the mass of the AGB component (which only impacts the current WD mass). Therefore, its value can simply be read off the $P_{\rm RGB,1}$ curve (bold dashed line) at the corresponding $M_{\rm Ba}$ value (although $P_{\rm RGB,1}$ and $P_{\rm RGB,1}$ are not strictly equal, they are not different enough to warrant a specific curve that would jeopardize the clarity of the figure; but see Table 3).

mass stars ($M/M_\odot < 2.5$) is consistent with our finding about the barium-star HRD, and in particular with the lack of systems with periods shorter than 1000 d among post-RGB-tip systems.

Another (apparent) puzzle emerges from this analysis: the fact that these critical periods at RGB tip are way shorter than the threshold imposed by the passage of the AGB companion through the AGB tip, which corresponds to periods in the range 1000 to 7500 d (thin lines in Fig. 16). Clearly, most of the barium systems have periods shorter than the critical periods at the AGB tip. Most should thus have gone through RLOF at AGB tip, and this RLOF cannot have led to a catastrophic outcome (coalescence or hour-long orbital periods like in cataclysmic variables). The key difference between RLOF close to AGB tip and to RGB tip is the mass of the residual envelope: it is generally large at the RGB tip, but must be much smaller at the AGB tip, since the AGB star is there almost reduced to its WD core. Hence, RLOF close to AGB tip does not involve a massive envelope, and the ensuing common envelope, if any, cannot be very massive thus. Therefore, any orbital shrinkage must be very modest as well. Alternatively, if RLOF starts

Table 3. The RGB-tip radius, luminosity and $T_{\rm eff}$ for stars of different masses, according to the STAREVOL evolutionary tracks (Siess 2006) for $Z = 0.0134$, and the corresponding critical period $P_{\rm RGB,2}$ (see text). The WD companion, with a mass of 0.61 $M_\odot$, is supposed to originate from a 3.1 $M_\odot$ AGB progenitor.

M ($M_\odot$)	$\log(L/L_\odot)$	$\log(T_{\rm eff})$	$R_{\rm RGBtip}$ ($R_\odot$)	a ($R_\odot$)	P (d)
1.1	3.42	3.47	194	450	839
1.5	3.44	3.51	169	368	559
1.9	3.44	3.53	154	322	420
2.5	3.61	3.53	183	364	454
3.1	2.91	3.61	56	108	67

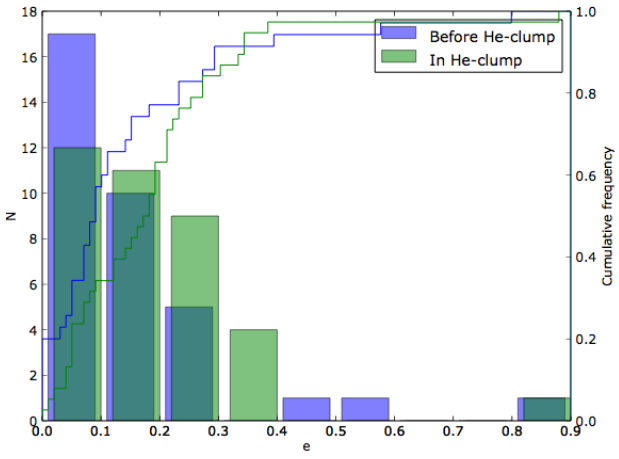

Fig. 17. Same as Fig. 15 for the orbital eccentricity.

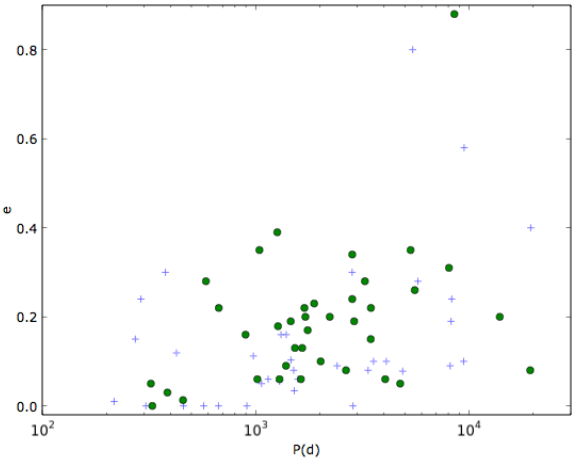

Fig. 18. The $e - P$ diagram for the same two subpopulations as in Fig. 17: blue crosses correspond to pre-He-clump systems and green dots to systems located at the He clump.

when the mass ratio has already been reversed, this situation does not lead to a dynamical mass transfer at all, since the orbital separation then expands.

A segregation similar to that observed in the post-RGB-tip HRD of barium stars must occur, though, for low-mass primary stars when they evolve along the RGB. This effect does introduce as well a true selection against barium systems with masses below 2.5 $M_\odot$ with initial periods shorter than 1000 d.

Fig. 17 is similar to Fig. 15, but for the orbital eccentricity. It reveals that the He-clump sample does not contain more systems with small eccentricities than the pre-He-clump sample (in fact it contains *less* systems with small eccentricities). This result is surprising since it suggests that the passage through the RGB-tip has not decreased the eccentricity, contrarily to what is expected if tidal effects dominate. In fact, the period – eccentricity diagram (Fig. 18) reveals that the larger average eccentricity of the He-clump systems is the result of the lack of short-period systems with low eccentricities, as observed among pre-He-clump systems (blue crosses in Fig. 18; the four green dots at short-period and low-eccentricities in that Fig. are probably systems that happen to fall among He-clump systems but which are on their way to the RGB tip; such a contamination must indeed be expected). Therefore, the lack of short-period, low-eccentricity systems among He-clump systems suggests that systems with periods shorter than about 1000 d (Table 3) have disappeared form the sample of barium stars, most likely because they went through RLOF and suffered from dramatic orbital shrinkage, or even coalesced. Since early R-type carbon stars are another family of peculiar stars with a strong concentration in the He clump (Knapp et al. 2001), and none is member of a binary system (McClure 1997), we tentatively suggest that the early R stars are coalesced systems corresponding to the missing short-period, post-RGB-tip barium systems. As may be inferred from Fig. 15, the pre-He-clump systems with periods shorter than 1000 d represent about 40% of the full sample, we expect that early R stars should have a Galactic frequency which is about half that of He-clump barium stars. Knapp et al. (2001) find about 30 early R-type carbon stars in a volume limited to 600 pc around the Sun. In the same volume, there are 102 He-clump barium stars with reliable distances (i.e., $\varpi/\sigma(\varpi) > 3$), and this sample is almost complete, as may be judged from Fig. 1 for $\varpi \geq 1.67$ mas. Thus the ratio of He-clump R stars to He-clump barium stars (30/102) matches, to within 10%, the prediction (40%) based on the fraction of systems with $P < 1000$ d among pre-He-clump systems. The hypothesis that the early R stars are coalesced systems corresponding to the missing short-period, post-RGB-tip barium systems is thus confirmed by this simple prediction of their respective frequencies. A similar hypothesis, although not backed up by the present frequencies, has already been suggested by different authors (e.g., Izzard et al. 2007; Zamora et al. 2009; Zhang & Jeffery 2013). The origin of R stars as final products of binary-star mergers is further supported by the fact that, except for BD +02°4338 reported as a long-period binary by Makarov & Kaplan (2005) and Frankowski et al. (2007), all early-R stars seem to be single stars (McClure 1997). The absence of evidence for the binary nature of the early R-type carbon stars has been confirmed from a precise monitoring with the HERMES spectrograph installed on the 1.2m Mercator telescope at the Roque de los Muchachos Observatory (Raskin et al. 2011). This will be further discussed in a companion paper about R stars (Knapp et al., in preparation).

The major problem with the hypothesis of a link between barium and R stars, however, is the lack of s-

process element overabundances in early R-type carbon stars (Zamora et al. 2009). Nevertheless, we conjecture that the s-process elements, formerly present in the envelope of the barium star, got so strongly diluted during the merger event that no overabundance remains in the resulting R carbon star. over the entire star, and is no more detectable, whereas some carbon could be produced during the event and dredged up to the surface (Izzard et al. 2007; Zhang & Jeffery 2013).

A second issue to be clarified is why barium systems do not suffer a cataclysmic fate on the AGB as R stars probably do on the RGB tip. Indeed, barium dwarfs with periods shorter than 1000 d do exist, and these evolve directly from the AGB. The question then is this: what distinguishes the evolution of a barium system along the RGB and along the AGB, to prevent a dramatic outcome associated with mass transfer on the AGB? The mass-ratio reversal that occurs easily on the AGB due to the strong mass-loss rate (thus making the mass-transferring AGB component less massive than its accreting companion, the future barium star) stabilizes mass transfer, thus preventing a dramatic fate. This situation is only rarely encountered during the RGB evolution (see, however, Siess et al. 2014, for an exception leading to the system IP Eri containing a He WD in a long-period system), because mass loss is very moderate on the RGB as compared to the AGB. Moreover, eccentricity pumping through either periastron mass transfer or circumbinary-disc tidal interactions (Dermine et al. 2013) is required to lead to short-period, large-eccentricity dwarf Ba systems as observed on Fig. 18.

****** And mild vs strong Ba ? ******

7. Conclusions

Acknowledgements. Gaia - DR1, PRODEX, Be-BRAIN, FWO, FNRS CQ

References

Baranne, A., Mayor, M., & Poncet, J. L. 1979, Vistas in Astronomy, 23, 279
Bartkevičius, A. 1996, Baltic Astronomy, 5, 217
Bensby, T. & Feltzing, S. 2006, MNRAS, 367, 1181
Bensby, T., Feltzing, S., & Oey, M. S. 2014, A&A, 562, A71
Bessell, M. S., Castelli, F., & Plez, B. 1998, A&A, 333, 231
Bidelman, W. P. & Keenan, P. C. 1951, 114, 473
Bond, J. C., Lauretta, D. S., Tinney, C. G., et al. 2008, ApJ, 682, 1234
Degroote, P., Acke, B., Samadi, R., et al. 2011, A&A, 536, A82
Dermine, T., Izzard, R. G., Jorissen, A., & Van Winckel, H. 2013, A&A, 551, A50
Edvardsson, B., Andersen, J., Gustafsson, B., et al. 1993, A&A, 275, 101
ESA. 1997, The Hipparcos and Tycho Catalogues (ESA)
Falcon, R. E., Winget, D. E., Montgomery, M. H., & Williams, K. A. 2010, ApJ, 712, 585
Famaey, B., Jorissen, A., Luri, X., et al. 2005, A&A, 430, 165
Frankowski, A., Jancart, S., & Jorissen, A. 2007, A&A, 464, 377
Gontcharov, G. A. 2012, Astronomy Letters, 38, 87
Høg, E., Fabricius, C., Makarov, V. V., et al. 2000, A&A, 355, L27
Izzard, R. G., Dermine, T., & Church, R. P. 2010, A&A, 523, A10
Izzard, R. G., Jeffery, C. S., & Lattanzio, J. 2007, A&A, 470, 661
Käppeler, F., Gallino, R., Bisterzo, S., & Aoki, W. 2011, Reviews of Modern Physics, 83, 157
Knapp, G., Pourbaix, D., & Jorissen, A. 2001, A&A, 371, 222
Kurucz, R. L. 1979, ApJS, 40, 1
Livio, M. 1994, in Interacting Binaries (Saas-Fee Advanced Course 22), ed. S. N. Shore, M. Livio, & E. van den Heuvel (Berlin: Springer-Verlag), 135
Lü, P. K. 1991, 101, 2229
Lü, P. K., Dawson, D. W., Upgren, A. R., & Weis, E. W. 1983, 52, 169
Luri, X. & Arenou, F. 1997, in ESA Special Publication, Vol. 402, Hipparcos - Venice '97, ed. R. M. Bonnet, E. Høg, P. L. Bernacca, L. Emiliani, A. Blaauw, C. Turon, J. Kovalevsky, L. Lindegren, H. Hassan, M. Bouffard, B. Strim, D. Heger, M. A. C. Perryman, & L. Woltjer, 449–452
Makarov, V. V. & Kaplan, G. H. 2005, AJ, 129, 2420
McClure, R. D. 1997, 109, 256
McClure, R. D., Fletcher, J. M., & Nemec, J. M. 1980, 238, L35
McClure, R. D. & Woodsworth, A. W. 1990, ApJ, 352, 709
Mennessier, M. O., Luri, X., Figueras, F., et al. 1997, A&A, 326, 722
Michalik, D., Lindegren, L., & Hobbs, D. 2015, A&A, 574, A115
North, P., Berthet, S., & Lanz, T. 1994, A&A, 281, 775
Pereira, C. B. 2005, AJ, 129, 2469
Pols, O. R., Karakas, A. I., Lattanzio, J. C., & Tout, C. A. 2003, in Symbiotic Stars Probing Stellar Evolution (ASP Conf. Proc. 303) (San Francisco: Astronomical Society of the Pacific), 290
Pourbaix, D. & Jorissen, A. 2000, A&AS, 145, 161
Raskin, G., van Winckel, H., Hensberge, H., et al. 2011, A&A, 526, A69
Siess, L. 2006, A&A, 448, 717
Siess, L., Davis, P. J., & Jorissen, A. 2014, A&A, 565, A57
Skrutskie, M. F., Cutri, R. M., Stiening, R., et al. 2006, AJ, 131, 1163
Van der Swaelmen, M., Boffin, H. M. J., Jorissen, A., & Van Eck, S. 2016, A&A, in press, arXiv 1608.04949
Warner, B. 1965, 129, 263
Webbink, R. F. 1988, in Critical Observations Versus Physical Models for Close Binary Systems, ed. K.-C. Leung, 403–446
Weingartner, J. C. & Draine, B. T. 2001, ApJ, 548, 296
Zamora, O., Abia, C., Plez, B., Domínguez, I., & Cristallo, S. 2009, A&A, 508, 909
Zhang, X. & Jeffery, C. S. 2013, MNRAS, 430, 2113